arXiv:0902.4568v2 [hep-ph] 8 May 2009

Mixed Neutralino Dark Matter in Nonuniversal Gaugino Mass Models

Utpal Chattopadhyay[(a)], Debottam Das[(a)] and D.P.Roy[(b)]

[(a)] *Department of Theoretical Physics, Indian Association for the Cultivation of Science, 2A & 2B Raja S.C. Mullick Road, Kolkata 700 032, India*

[(b)] *Homi Bhabha centre for Science Education, Tata Institute of Fundamental Research, V.N. Purav Marg,Mumbai-400088,India*

Abstract

We have considered nonuniversal gaugino mass models of supergravity, arising from a mixture of two superfield contributions to the gauge kinetic term, belonging to a singlet and a nonsinglet representation of the GUT group. In particular we analyse two models, where the contributing superfields belong to the singlet and the 75-dimensional, and the singlet and the 200-dimensional representations of SU(5). The resulting lightest superparticle is a mixed bino-higgsino state in the first case and a mixed bino-wino-higgsino state in the second. In both cases one obtains cosmologically compatible dark matter relic density over broad regions of the parameter space. We predict promising signals in direct dark matter detection experiments as well as in indirect detection experiments via high energy neutrinos coming from their pair-annihilation in the Sun. Besides, we find interesting γ-ray signal rates that will be probed in the Fermi Gamma-ray Space Telescope. We also expect promising collider signals at LHC in both cases.

PACS No: 04.65.+e, 13.40Em, 14.60Ef, 13.85.-t, 14.80.Ly

1 Introduction

A leading candidate for the cold dark matter of the universe is the lightest supersymmetric particle (LSP) of the minimal supersymmetric standard model (MSSM) [1]. Astrophysical constraints require the LSP to be colorless and chargeless, while direct dark matter (DM) search experiments strongly disfavour a sneutrino LSP. Thus the favoured candidate for LSP in the MSSM is the lightest neutralino

$$\tilde{\chi} \equiv \tilde{\chi}_1^0 = c_1\tilde{B} \ + c_2\tilde{W}^3 \ + c_3\tilde{H}_D^0 \ + c_4\tilde{H}_U^0. \tag{1}$$

The neutralino mass matrix is given by

$$M_N = \begin{pmatrix} M_1 & 0 & -M_Z \cos\beta \sin\theta_W & M_Z \sin\beta \sin\theta_W \\ 0 & M_2 & M_Z \cos\beta \cos\theta_W & -M_Z \sin\beta \cos\theta_W \\ -M_Z \cos\beta \sin\theta_W & M_Z \cos\beta \cos\theta_W & 0 & -\mu \\ M_Z \sin\beta \sin\theta_W & -M_Z \sin\beta \cos\theta_W & -\mu & 0 \end{pmatrix}, \tag{2}$$

where M_1,M_2 and μ are the bino,wino and higgsino mass parameters; and $\tan\beta$ represents the ratio of two Higgs vacuum expectation values. The LSP is the lightest eigenstate of the mass matrix. It can be a dominantly bino,wino or higgsino state or else a large admixture of these interaction eigenstates.

Much of the MSSM phenomenology so far has been done in the context of minimal supergravity (mSUGRA) [2] model, because of its simplicity and economy of parameters. This model predicts a dominantly bino LSP over the bulk of the parameter space. The bino does not couple to gauge bosons since it does not carry any gauge charge. So the main annihilation mechanism of the bino dark matter is via t-channel slepton exchange, $\tilde{\chi}\tilde{\chi} \xrightarrow{\tilde{l}} l^+l^-$. However the large slepton mass limits from LEP [3], particularly in the mSUGRA model, makes this annihilation mechanism inefficient. This leads to a gross overabundance of the DM relic density over the bulk of the mSUGRA parameter space. There are only narrow strips of parameter space, like the stau coannihilation ($\tilde{\chi}\tilde{\tau} \xrightarrow{\tau} \tau\gamma$) and resonant annihilation ($\tilde{\chi}\tilde{\chi} \xrightarrow{A} b\bar{b}, t\bar{t}, \tau^+\tau^-$) regions giving cosmologically compatible DM relic density [4] which require however some stringent mass correlations between the annihilating LSPs and the intermediate particle in the s-channel resonance or between a coannihilating sparticle and the LSP.

In contrast, the higgsino and wino carry weak isospin $I = \frac{1}{2}$ and 1 respectively. So a higgsino and wino-dominated LSP can pair-annihilate efficiently via their couplings to the W/Z gauge bosons, leading to an underabundance of DM relic density for sub-TeV LSP masses. One can get cosmologically compatible relic density only for relatively large LSP masses of $M_{\tilde{H}} \simeq 1$ TeV and $M_{\tilde{W}} \simeq 2$ TeV, which make these models inaccessible to LHC. They can only be probed at a multi-TeV linear collider like CLIC [5, 6].

It is evident from the above discussion that a mixed bino-higgsino or bino-wino LSP is expected to give cosmologically compatible DM relic density for sub-TeV LSP masses, which can be probed at the LHC. This has been described as the 'well-tempered' scenario

in Ref. [7]. The DM relic density and the detection phenomenology of this scenario have been studied in a model independent way in Ref. [8]. It should be mentioned here that a very important example of the mixed bino-higgsino LSP occurs in the so-called hyperbolic branch/focus point (HB/FP) [9–12] region of mSUGRA model. This is a narrow strip at the edge of the mSUGRA parameter space, corresponding to very large (multi-TeV) scalar masses.

In this work, we investigate a class of nonuniversal gaugino mass models, where the mixed neutralino LSP can be realised in a simple and economical way. In particular we construct two models − the first giving a mixed bino-higgsino LSP and the second giving a mixed bino-wino LSP. The latter model also gives a triply mixed bino-wino-higgsino LSP over a significant part of the parameter space. For each of these two models we find cosmologically compatible DM relic density over broad bands passing through the middle of the parameter space in the $m_0 - m_{\frac{1}{2}}$ plane. We also investigate the expected signals in both cases for direct and indirect DM detection experiments. In each case we find promising signals for future direct detection experiments. Likewise we find promising indirect detection signals in each case for the IceCube experiment, in the form of high energy neutrinos coming from DM pair-annihilation inside the Sun. We also estimate the corresponding line and continuum γ ray signals coming from their pair-annihilation in the galactic core. We conclude with a brief discussion of the expected collider signatures of these models at LHC.

2 Nonuniversal Gaugino Mass Models for mixed neutralino DM:

SUGRA models with nonuniversal gaugino masses at the GUT scale have been studied in many earlier works [13–21]. We shall only summarize the main results here, focusing on the simplest and most predictive GUT group, $SU(5)$. Here the gauge kinetic function that is related to the GUT scale gaugino masses, arises from the vacuum expectation value of the F-term of a chiral superfield Φ, which is responsible for SUSY breaking. This results in a dimension five term in the lagrangian,

$$L \supset \frac{< F_\Phi >_{ij}}{M_{Planck}} \lambda_i \lambda_j, \tag{3}$$

where $\lambda_{1,2,3}$ are the $U(1)$, $SU(2)$ and $SU(3)$ gaugino fields − bino ($\tilde{B}$), wino ($\tilde{W}$) and gluino ($\tilde{g}$). Since the gauginos belong to the adjoint representation of $SU(5)$, Φ and F_Φ can belong to any of the irreducible representations appearing in their symmetric product, i.e.

$$(24 \times 24)_{symm} = 1 + 24 + 75 + 200. \tag{4}$$

The minimal SUGRA model assumes Φ to be a singlet, implying equal gaugino masses at the GUT scale. On the other hand if Φ belongs to one of the nonsinglet representations of $SU(5)$, then these gaugino masses are unequal but related to one another via the representation invariants. Thus the three gaugino masses at the GUT scale in a given representation n are determined in terms of a single SUSY breaking mass parameter $m^n_{1/2}$ by

$$M^G_{1,2,3} = C^n_{1,2,3} m^n_{1/2}, \tag{5}$$

where

$$C^1_{1,2,3} = (1,1,1),\ C^{24}_{1,2,3} = (-1,-3,2),\ C^{75}_{1,2,3} = (-5,3,1),\ C^{200}_{1,2,3} = (10,2,1). \tag{6}$$

The nonuniversal gaugino mass models are known to be consistent with the observed universality of the gauge couplings at the GUT scale [13, 15], with $\alpha^G (\simeq 1/25)$. Since the gaugino masses evolve like the corresponding gauge couplings at one-loop level of the renormalisation group equations (RGE), the three gaugino masses at the electroweak (EW) scale are proportional to the corresponding gauge couplings, i.e.

$$\begin{aligned} M_1 &= (\alpha_1/\alpha_G) M^G_1 \simeq (25/60) C^n_1 m^n_{1/2} \\ M_2 &= (\alpha_2/\alpha_G) M^G_2 \simeq (25/30) C^n_2 m^n_{1/2} \\ M_3 &= (\alpha_3/\alpha_G) M^G_3 \simeq (25/9) C^n_3 m^n_{1/2}. \end{aligned} \tag{7}$$

For simplicity we shall assume a universal SUSY breaking scalar mass m_0 at the GUT scale. Then the scalar masses at the electroweak scale are given by the renormalisation group evolution formulae [22, 23]. A very important SUSY breaking mass parameter at this scale is $m^2_{H_U}$, which appears in the EW symmetry breaking condition,

$$\mu^2 + M^2_Z/2 = \frac{m^2_{H_D} - m^2_{H_U} \tan^2\beta}{\tan^2\beta - 1} \simeq -m^2_{H_U}. \tag{8}$$

The last equality holds for the $\tan\beta \geq 5$ region, which is favoured by the Higgs mass limit from LEP2 [24]. Expressing $m^2_{H_U}$ at the right in terms of the GUT scale parameters via the one-loop RGE gives [23]

$$\begin{aligned}\mu^2 + \frac{1}{2}M_Z^2 \;\simeq\; & -0.1m_0^2 + 2.1M_3^{G2} - 0.22M_2^{G2} - 0.006M_1^{G2} + 0.006M_1^G M_2^G + \\ & 0.19M_2^G M_3^G + 0.03M_1^G M_3^G, \end{aligned} \tag{9}$$

at a representative value of $\tan\beta = 10$, neglecting the contribution from the trilinear coupling term at the GUT scale. Moreover, the coefficients vary rather mildly over the moderate $\tan\beta$ region.

Although we shall use exact numerical solutions to the two-loop RGE in our analysis, one important result is worth noting from the simple formulae of Eqs. (5,6,7,9). For the singlet and 24-plate representations of the SUSY breaking chiral superfield Φ, we have $|M_1| < |M_2|, |\mu|$. This corresponds to a bino LSP, resulting in overabundance of DM relic density over most of the parameter space. On the other hand, for the 75-plate and 200-plate representations we get $|\mu| < |M_1|, |M_2|$. This corresponds to a higgsino LSP, resulting in underabundance of DM relic density [17].

In general the gauge kinetic function may contain several chiral superfields, belonging to different representations of $SU(5)$, which gives us the freedom to vary the relative magnitudes of M_1,M_2 and μ continuously. In particular we shall consider two models, where the gauge kinetic function contains a mixture of singlet plus 75-plet superfields $(1 + 75)$ in the first case and a singlet plus 200-plet superfields $(1 + 200)$ in the second. By adjusting the relative contribution from the two superfields we shall obtain a mixed bino-higgsino LSP in the first case and a mixed bino-wino LSP in the second, each giving favourable DM relic density over large regions of the parameter space. It should be mentioned here that mixtures of singlet and nonsinglet superfield contributions were first discussed in Ref. [13]. Moreover, the $(1 + 24)$, (1+75) and (1+200) models were considered in the context of i) direct detection of neutralino DM in Ref. [14], and ii) a bino DM in Ref [18], where in the latter the relative contribution from the two superfields were adjusted to recover the bulk annihilation region of the right DM relic density in each case. Nonuniversal gaugino mass models based on such mixed representations have also been considered more recently to investigate the Higgs production phenomenology via SUSY cascade decay [20]. To the best of our knowledge however, this is the first investigation of such nonuniversal gaugino mass models, to obtain the right relic

density via mixed neutralino DM. As in [18], we shall vary the relative contribution of the two superfields via a single parameter, i.e

$$m^1_{1/2} = (1-\alpha_{75})m_{1/2} \quad \text{and} \quad \mathrm{m}^{75}_{1/2} = \alpha_{75}\mathrm{m}_{1/2}, \tag{10}$$

for the (1+75) model and

$$m^1_{1/2} = (1-\alpha_{200})m_{1/2} \quad \text{and} \quad \mathrm{m}^{200}_{1/2} = \alpha_{200}\mathrm{m}_{1/2}, \tag{11}$$

for the (1+200) model. Then one sees from Eqs. (5,6,7,9) that for the (1+75) model,

$$\alpha_{75} \equiv 0.50 \Longrightarrow |M_1| \simeq |\mu| \simeq m_{1/2} < |M_2| \tag{12}$$

for $m_0 \geq m_{1/2}$. This leads to a mixed bino-higgsino LSP. One also sees from Eq. (9) that decreasing m_0 leads to increase of $|\mu|$ and hence decrease of higgsino fraction of LSP. Moreover one sees from eqns (5,6,7) that for (1+200) model

$$\alpha_{200} \equiv 0.1 \Longrightarrow |M_1| \simeq |M_2|, \tag{13}$$

leading to a mixed bino-wino LSP. Again one sees from equation (9) that increasing m_0 leads to decrease of $|\mu|$, resulting in a triply mixed bino-wino-higgsino LSP in the large m_0 region. We shall present the results for the $(1+75)$ and $(1+200)$ models in the following sections.

α_{75}	$\lvert M_1\rvert$	μ	α_{200}	M_1	M_2	μ
-	(GeV)	(GeV)	-	(GeV)	(GeV)	(GeV)
0.3	177	552	0.1	400	442	612
0.4	307	519	0.12	439	451	611
0.45	372	495	0.15	496	463	609
0.475	404	484	0.2	592	483	604
0.5	437	473	0.3	783	523	593
0.55	502	448	0.45	1073	584	568

Table 1: Variation of mass parameters with α_{75} (for the (1+75) model) and α_{200} (for the (1+200) model) for $m_0 = m_{1/2} = 500$ GeV, $A_0 = 0$,$\tan\beta = 10$, and sign$(\mu) = +$ve.

We have probed how the nature of the LSP varies with the choice of mixing parameters in Table 1. We show M_1 and μ for a few values of α_{75} for the (1+75) model for a given

set of other parameters. Similarly we show M_1, M_2 and μ for a few values of α_{200} for the (1+200) model. One can infer the dominant component of the LSP from the relative values of these masses. In the (1+75) model, the LSP is dominantly bino for $\alpha_{75} \leq 0.45$, leading to a generic overabundance of DM. On the other hand it is dominantly higgsino for $\alpha_{75} \geq 0.55$, leading to a generic underabundance of DM. In the (1+200) model, the LSP is dominantly wino for $\alpha_{200} \geq 0.15$, becoming dominantly higgsino for $\alpha_{200} \geq 0.45$. There is a generic underabundance of DM throughout the wino/higgsino dominated LSP region of $\alpha_{200} \geq 0.15$. On the other hand, $\alpha_{200} < 0.1$ results in a dominant bino content of the LSP leading to a generic overabundance of DM.
Thus we have found the optimised mixing parameters to be

$$\alpha_{75} = 0.475 \quad \text{and} \quad \alpha_{200} = 0.12 \tag{14}$$

so as to get the most favourable DM relic density. There is admittedly some finer adjustment involved in these parameters so that we may be able to probe such large mixing zones of LSP. This is analogous to the delicate correlations between the mass parameters existing in the stau coannihilation or the resonant annihilation regions that provide with cosmologically favourable DM relic density in mSUGRA models, as pointed out in Section 1.

Note however that once the mixing parameter is so adjusted, then the $(1 + 75)$ and $(1 + 200)$ models are each as predictive as the mSUGRA model. Note that in the first case we need roughly equal contributions from the singlet and the 75-plet superfields to achieve a favourable DM relic density, while in the second case it is achieved through a dominantly singlet contribution with only $\sim 10\%$ admixture from the 200-plet superfield.

3 DM Relic Density for the $(1 + 75)$ Model:

We have computed the DM relic density for the $(1+75)$ and $(1+200)$ models in terms of the GUT scale mass parameters m_0 and $m_{1/2}$ using SUSPECT [25] for the numerical evaluation of the two-loop RGEs. The DM relic density was evaluated using micrOMEGAs [26] and cross-checked with DARKSUSY [27].

Fig.1 shows the DM relic density in the $m_0 - m_{1/2}$ plane for the $(1 + 75)$ model with the mixing parameter of eq.(14) and a moderate value of $\tan\beta = 10$. For simplicity we have set $A_0 = 0$ and positive μ. The upper disallowed region (in gray) corresponds to the lighter

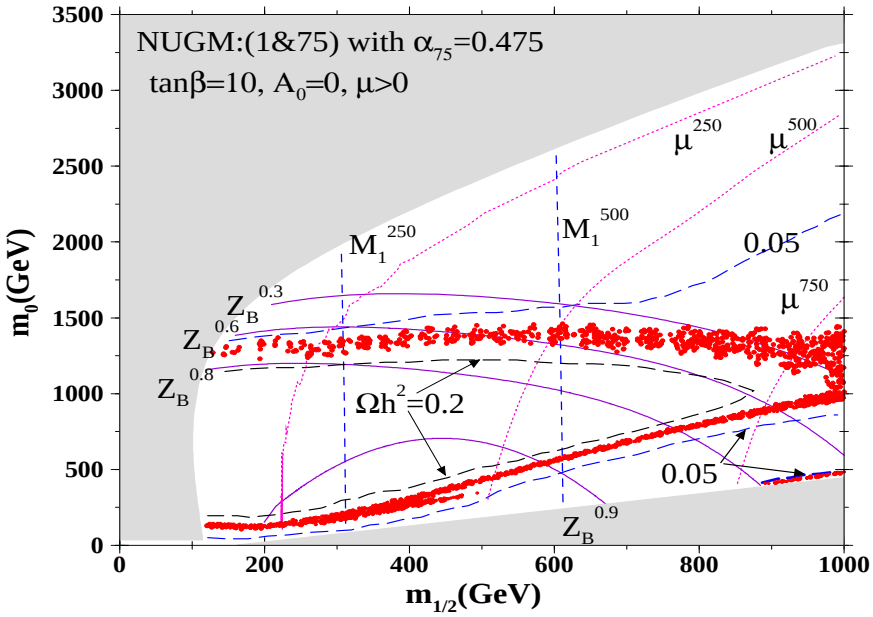

Figure 1: Allowed and disallowed zones of the $(1+75)$ model. The WMAP DM relic density satisfying regions are shown in red in the $m_0 - m_{1/2}$ plane for $\tan\beta = 10$, $A_0 = 0$, $\mu > 0$ corresponding to $\alpha_{75} = 0.475$ of Eq.14. The upper disallowed region (in gray) corresponds to no EWSB ($\mu^2 < 0$). The lower gray region corresponds to stau becoming the LSP. Contours are drawn for M_1, μ, Z_B and $\Omega_{CDM}h^2$.

chargino being smaller than the LEP limit [3] or no EWSB ($\mu^2 < 0$); and the lower one to a stau LSP. The allowed region is mapped by constant M_1 and μ contours. At the intersection points $M_1 = \mu$, the LSP is an equi-mixture of bino and higgsino ($Z_B \equiv c_1^2 = 0.5$). The bino fraction increases with decreasing m_0, as indicated by the fixed Z_B contours. The region satisfying the DM relic density value of the WMAP data [4]

$$\Omega_{CDM}h^2 = 0.1099 \quad \pm 0.0186\ (3\sigma), \tag{15}$$

is indicated by the bands of red dots. The contours of fixed $\Omega_{CDM}h^2 = 0.05$ and 0.2 are also shown on the two sides of these red bands.

We see from Fig.1 that almost half the parameter space corresponds to DM relic density being in the right ball-park of $\Omega_{CDM}h^2 = 0.05 - 0.2$. And even the precise WMAP value of Eq.(15) is satisfied by two fairly thick bands passing through the middle of the parameter space. The upper band corresponds to the DM being a roughly equal admixture of $\tilde{B} - \tilde{H}$,

parameter	A	B	C	D	E	F
$m_{1/2}$	300	600	800	300	600	800
m_0	1325	1400	1340	185	550	800
μ	268	496	654	323	560	694
M_1	242	493	662	237	489	660
$m_{\tilde{\chi}_1^0}$	227	468	631	231	481	645
$m_{\tilde{\chi}_2^0}$	254	489	649	302	552	689
$m_{\tilde{\chi}_3^0}$	289	524	687	334	571	711
$m_{\tilde{\chi}_4^0}$	501	970	1285	490	957	1277
$m_{\tilde{\chi}_1^+,\tilde{\chi}_2^+}$	255,501	490,970	649,1285	304,491	552,957	689,1277
$m_{\tilde{g}}$	794	1437	1845	725	1381	1809
$m_{\tilde{t}_1}$	903	1232	1435	485	965	1280
$m_{\tilde{t}_2,\tilde{b}_1}$	1256,1246	1704,1694	1993,1983	727,651	1367,1288	1800,1712
$m_{\tilde{l}}$	1300−1400	1400−1600	1440−1680	280−440	680−950	960−1300
$m_{\tilde{q}_{1,2}}$	1400−1500	1800−1940	2000−2220	650−750	1300−1480	1725−1965
$m_A(\simeq m_{H^+}, m_H)$	1382	1648	1786	534	1091	1460

Table 2: MSSM masses in GeV for a few sample parameter points for the $1 + 75$ model.

where their pair-annihilation occurs mainly via the gauge coupling of the higgsino component. With decreasing m_0 the bino component (Z_B) increases, leading to the increase of DM relic density upto $\Omega_{CDM}h^2 \simeq 0.6$. However further decrease of m_0 leads to resonant pair-annihilation via the pseudo-scalar higgs boson A, as $2M_1 \to m_A$. This is the dominant dark matter annihilation mechanism for the lower red band, satisfying the WMAP relic density of Eq. (15). The region below this band has an underabundance of DM relic density because of the resonant pair annihilation as $m_A \simeq 2M_1$. This is the so-called funnel region. The lower edge of the funnel is marked by the red strip at the bottom right, adjacent to the lower boundary. We have found this strip to be dominated by resonant pair annihilation of DM via A, with only $\sim 10\%$ contribution from the stau coannihilation. The $\Omega_{CDM}h^2 \simeq 0.05$ contour (its lower branch) practically overlaps with the upper edge of this red strip.

Table 2 lists the SUSY spectra for three representative points on each of the two main branches, satisfying DM relic density from WMAP(Eq.15). Note that the SUSY spectra show an inverted mass hierarchy , where the lighter stop($\tilde{t}_1$) is much smaller than the other

squark masses. This is related to the large negative contribution from the terms associated with top-Yukawa coupling in the renormalisation group evolution of the third generation of squark masses [11]. This feature is more pronounced for the upper branch, represented by the first three columns due to larger values of m_0. But it is quite significant for the lower branch as well. Note also an approximate degeneracy among the three lighter neutralinos ($\chi^0_{1,2,3}$) and the lighter chargino ($\tilde{\chi}^+_1$). This is again more prominent for the upper branch, which corresponds to a larger mixing between higgsinos and bino. Consequently, the coannihilation of χ^0_1 with χ^0_2 and $\tilde{\chi}^\pm_1$ make important contributions to the annihilation process. The dominant annihilation processes for the upper branch are

$$\chi^0_1\chi^0_1,\ \chi^0_1\chi^0_2,\ \chi^0_1\tilde{\chi}^\pm_1 \quad \rightarrow \quad WW,\ ZZ,\ f\bar{f}\ (\text{both via s and t} - \text{channel processes}) \tag{16}$$

which are driven by the gauge coupling of the higgsino component. On the other hand the lower branch is dominated by the resonant annihilation processes

$$\chi^0_1\chi^0_1,\ \chi^0_1\chi^0_2,\ \chi^0_1\tilde{\chi}^+_1 \quad \rightarrow \quad t\bar{t},\ b\bar{b}, \tau\bar{\tau},\ t\bar{b},\ \tau\nu_\tau\ (\text{via s} - \text{channel A}, \text{H}, \text{H}^+). \tag{17}$$

Since the gauge coupling of W/Z to the LSP pair goes like the square of its higgsino component, the annihilation process of Eq.16 are strongly suppressed with the decrease of the higgsino component to $\sim 10\%$ for the lower branch. On the other hand the A coupling to the LSP pair goes like the product of its higgsino and gaugino components and hence remains significant for a higgsino component of $\sim 10\%$. Even more importantly there is a large resonance enhancement for this region as $2m_{\chi^0_1} \rightarrow m_A$. This also includes some amount of coannihilation of χ^0_1 and χ^+_1 in the s-channel.

Note finally that a higgsino component of $\sim 10\%$ in the LSP is still large compared to the mSUGRA model except a few regions like HB/FP zones. This is why one can get a resonant annihilation region here even for a moderate value of $\tan\beta$ [28].

4 Direct & Indirect Detection rates for the $(1 + 75)$ Model:

We have estimated the DM signals for the $(1 + 75)$ model for direct and indirect detection experiments using the DARKSUSY [27]. The direct detection signal is based on the elastic

scattering of the DM on a heavy nucleus like Germanium or Xenon. The main contribution comes from the spin-independent interaction of the DM χ_1^0 with nucleon, which adds coherently in the nucleus. This is dominated by the Higgs exchange. Fig.2(a) shows the scatter plot of this cross-section against the DM mass. The discovery limits of present and proposed direct detection experiments are also shown for comparison. We have shown the limits from CDMS (Ge) 2005 [29], XENON-10 [30] and future SuperCDMS (Snolab) [31] and XENON1T [32] experiments in the figure. The upper and lower shaded (red) branches correspond respectively to the upper and lower WMAP relic density satisfying branches of Fig.1. Since the Higgs coupling to the neutralino DM is proportional to the product of its higgsino and gaugino components, one gets a larger cross-section for the upper branch of Fig.2(a), where DM corresponds to a roughly equal admixture of bino and higgsino. This comes within the detection limit of the proposed SuperCDMS experiment [31]. Both the branches will be covered by the proposed 1-Ton Xenon [32] experiment. Note that these cross-sections are larger than those of the mSUGRA model except the focus point region.

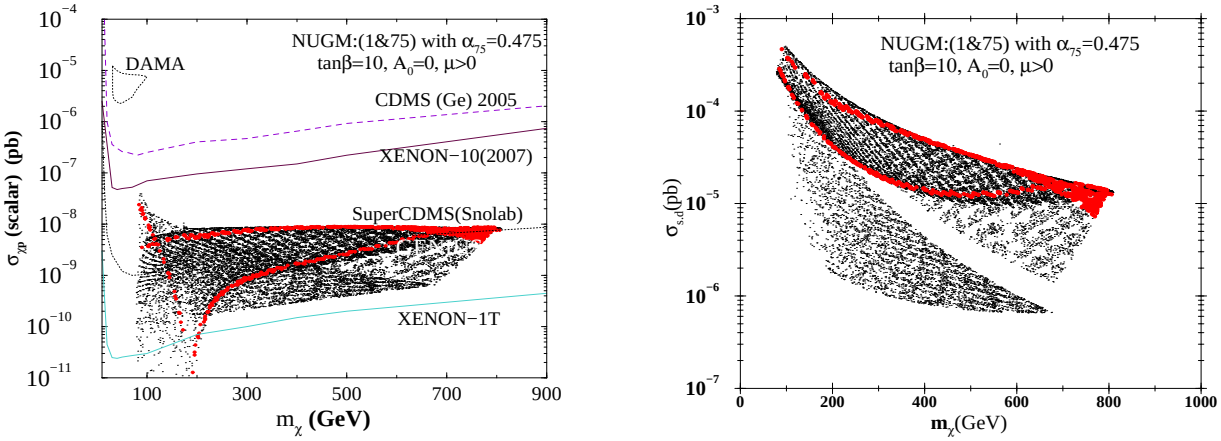

(a) (b)

Figure 2: (a): Spin-independent neutralino-proton cross section for the $(1 + 75)$ model vs. LSP mass for the parameters shown in Fig.1. The WMAP satisfied regions are shown in red. Various limits from the recent (DAMA, CDMS and XENON-10) and the future (SuperCDMS and XENON-1T) experiments are shown. (b): Spin-dependent neutralino-proton cross section for the $(1 + 75)$ model vs. LSP mass for the parameters shown in Fig.1. The WMAP satisfied regions are shown in red.

Fig.2(b) shows the corresponding scatter plot of the spin-dependent cross-section, which is dominated by Z exchange. Again upper and lower shaded (red) branches correspond to

WMAP satisfying branches of Fig.1 respectively. Since the Z coupling to the neutralino DM is proportional to the square of its higgsino component, one gets a larger cross-section for the upper branch of Fig.1, corresponding to a larger higgsino component of DM. The spin-dependent cross-sections in this model are significantly larger than those of the mSUGRA model (except the focus point region). But still they are much below the detection limits of any present or proposed direct detection experiments [33].

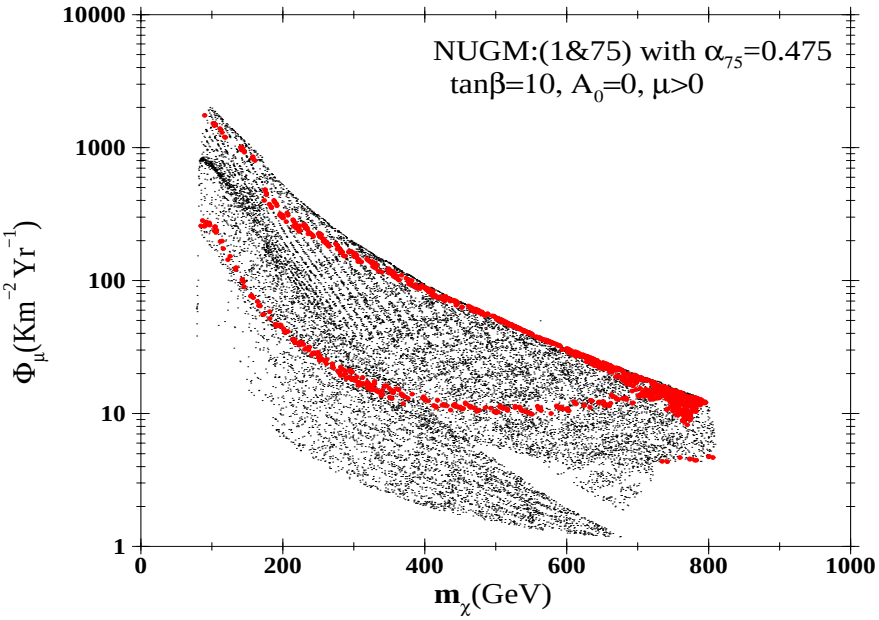

Figure 3: Neutralino annihilation induced muon flux from the Sun in $km^{-2}yr^{-1}$ vs LSP mass for the $(1+75)$ model for the parameters shown in Fig.1. The WMAP satisfied regions are shown in red.

A very promising indirect detection experiment for DM is via the high energy neutrinos coming from their pair-annihilation in the solar core. Since the annihilation rate at equilibrium is balanced by the DM capture rate inside the Sun, the resulting neutrino signal is proportional to the $\chi_1^0 - p$ cross-section. This is dominated by the above-mentioned spin-dependent interaction via Z exchange. Fig.3 shows the model prediction for the rate of muon signal events, resulting from these high energy neutrinos, in a km^2 size neutrino telescope like IceCube [34]. Again upper and lower shaded (red) branches correspond to the upper and lower WMAP satisfying branches of Fig.1. One can even see a small red strip at the right end, corresponding to a similar one in Fig.1. One sees a very promising signal with

≥ 10 events/year at the IceCube. Since the Z coupling to the neutralino DM goes like the square of its higgsino component, the size of this signal is much larger than that of the bino dominated DM of the mSUGRA model.

We have also computed the high energy γ-ray signal coming from the pair annihilation of the DM at the galactic core, assuming the standard NFW profile of DM distribution near the galactic core [35]. Fig.4(a) shows the signal rate of line γ-rays coming from the DM pair annihilation, $\tilde{\chi}\tilde{\chi} \to \gamma\gamma(\gamma Z)$ with $E_\gamma \simeq m_\chi$ via W-boson loop. Again this decay amplitude is proportional to the square of the higgsino component of the neutralino DM. Consequently the upper and lower shaded (red) branches correspond to the respective WMAP satisfying branches of Fig.1, while the small red strip at the right end correspond to the corresponding one of Fig.1.

Fig.4(b) shows the signal rate of continuum γ-rays coming from the tree level pair annihilation processes of Eq.16 and Eq.17. Production of neutral pions and their subsequent decays into photons is the most important mechanism for this signal [37]. While the $b\bar{b}$ channel is the most prominent channel for the continuum γ-rays signal, the WW and ZZ channels are also very significant. The two shaded (red) bands of Fig.4(b) correspond to the two WMAP relic density satisfying bands of Fig.1. The isolated red strip on the top right corresponds to that on the bottom right of Fig.1, which is dominated by the $b\bar{b}$ channel. Finally Fig.4(c) shows the continuum γ-ray spectrum for some representative points of this model, along with the discovery limit of the Fermi Gamma-ray Space Telescope (FGST) experiment or formerly known as GLAST [38, 39]. One would need a boost[1] factor of $\sim 10^2$ to see this γ-ray signal in FGST/GLAST. Note however that one can raise (lower) the signal rate by a factor of $\sim 10^3$ by assuming a more spiked (flat) DM profile like that of Moore profile [41] (or a spherically symmetric isothermal core profile [42]).

5 DM Relic Density for the $(1 + 200)$ Model:

Fig.5 shows the DM relic density in the $m_0 - m_{1/2}$ plane for the $(1 + 200)$ model with the mixing parameter of eq.(14). Again the upper and lower disallowed regions corresponds

[1]Processes like adiabatic compression may cause a large enhancement of the DM density near the galactic center (see e.g. [36]). Larger DM annihilation rate may also result from existence of clumps within the halos of galaxies [40]. A boost factor essentially estimates a few such effects.

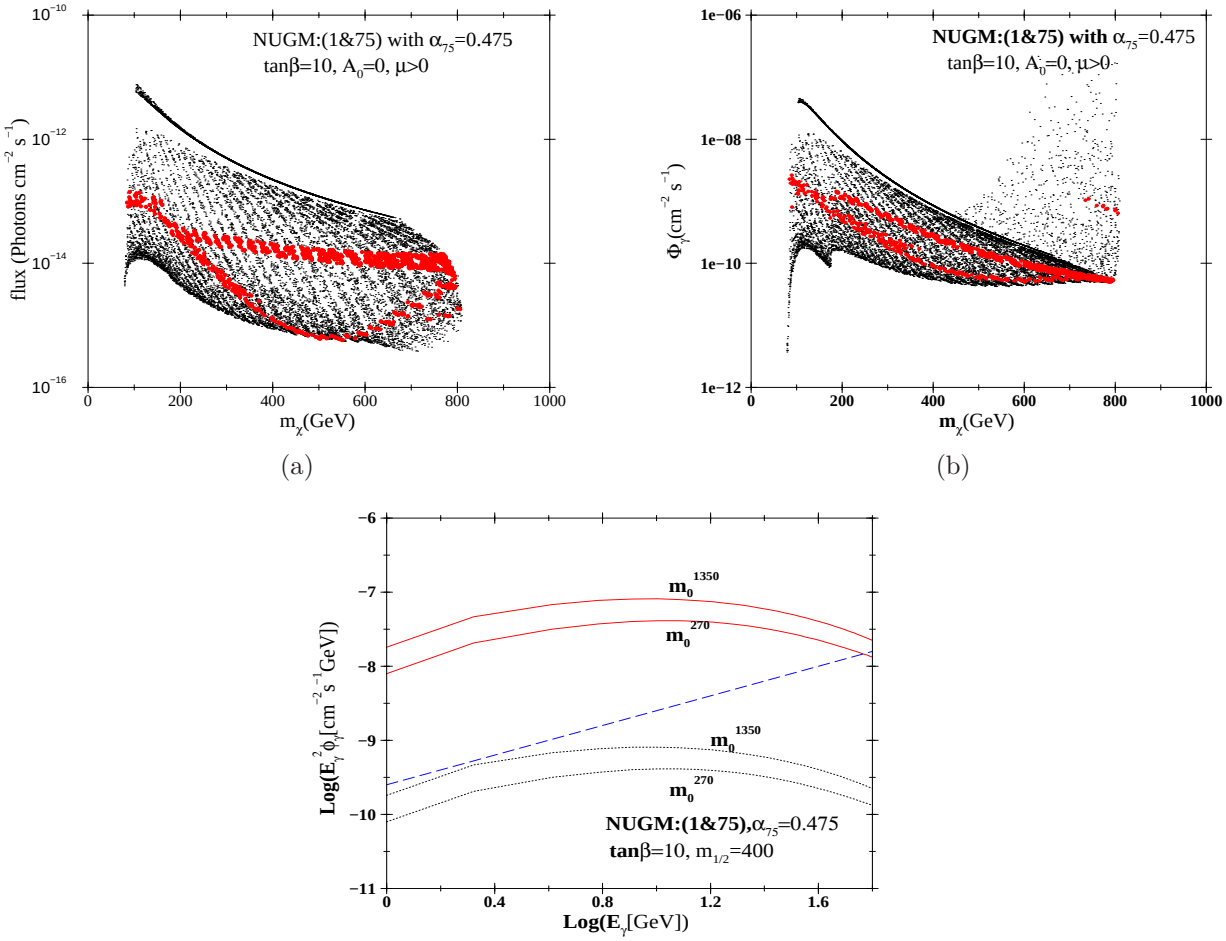

Figure 4: (a):Monochromatic γ-ray flux from DM pair annihilation near the galactic center vs. the LSP mass shown for the NFW profile of DM halo distribution and an aperture size of $\Delta\Omega = 10^{-3}$ sr for the $(1+75)$ Model. The parameters are same as in Fig.1. The WMAP satisfied regions are shown in red. (b): Same as (a) except that the vertical axis refers to a continuous γ-ray flux above a threshold energy of 1 GeV. (c): Photon spectra expected from two particular LSPs corresponding to $m_0 = 270$ GeV and $m_0 = 1350$ GeV for the $(1+75)$ Model with $m_{\frac{1}{2}} = 400$ GeV for an NFW profile. The other parameters are same as in Fig.1. The upper set of curves corresponds to a boost [36] factor of 10^2. The discovery limit of FGST/GLAST is shown as a blue straight line.

no EWSB ($\mu^2 < 0$); and to a stau LSP respectively. The allowed region is mapped by constant M_1 and M_2 along with the constant μ contours. We see from these contours

that the LSP is an equimixture of bino and wino ($\tilde{B}$-$\tilde{W}$), along with a significant higgsino component in the $m_0 > 1$ TeV region. In fact the intersection points of these contours ($M_1,\ M_2,\ \mu = 500$ and 800 GeV) mark the region of equally mixed $\tilde{B}$-$\tilde{W}$-$\tilde{H}$ LSP. The combined gaugino component of the LSP is indicated by the fixed $Z_g(\equiv c_1^2 + c_2^2)$ contours. This, when subtracted from unity would be a measure of the higgsino component. The region satisfying the DM relic density value of Eq.15 from WMAP is indicated by the bands of red dots. We see two thick bands in the middle of the parameter space. Note that these DM relic density satisfying bands correspond to LSP mass ≥ 500 GeV. The contours of fixed $\Omega_{CDM}h^2 = 0.05$ and 0.15 are also shown on the two sides of these red bands. The bulk of the parameter space outside these red bands corresponds to underabundance of DM relic density. In particular the corridor cutting through the two bands correspond to underabundance due to rapid resonant annihilation of DM pair via A-boson (i.e. the funnel region). For a clearer understanding of this model we list the SUSY spectra for two representative points from each of the two DM relic density satisfying branches in Table 3. This model requires a rather heavy SUSY spectrum for satisfying the DM relic density constraint. Note that the SUSY spectra of this model show an inverted mass hierarchy like the previous model, where the lighter stop ($\tilde{t}_1$) is significantly lighter than the other squarks. Note also the close degeneracy among the lighter neutralino and chargino states ($\chi^0_{1,2}$ and $\tilde{\chi}^+_1$) due to large bino-wino mixing. Therefore the coannihilation of χ^0_1 with χ^0_2 and $\tilde{\chi}^\pm_1$ make important contributions to the annihilation process as in the previous case. Both the branches are dominated by the annihilation process of Eq.16, driven by the gauge coupling of the wino (along with that of higgsino at large m_0). But there is a $30 - 40\%$ contribution coming from the resonant annihilation processes of Eq.17 on the strips adjacent to the 'funnel' corridor, where $2m_{\chi^0_1} \to m_A$. Note that the higgsino component of the LSP in this region is $\geq 10\%$, which is large enough for resonant annihilation via A even for a moderate value of $\tan\beta$ ($= 10$).

6 Direct & Indirect Detection rates for the $(1 + 200)$ Model:

Fig.6(a) shows the spin-independent scattering cross-section of the DM on nucleon, which gives the direct detection signal. The shaded (red) region covers the two WMAP relic density satisfying branches of Fig.5. Most of this region corresponds to the upper branch

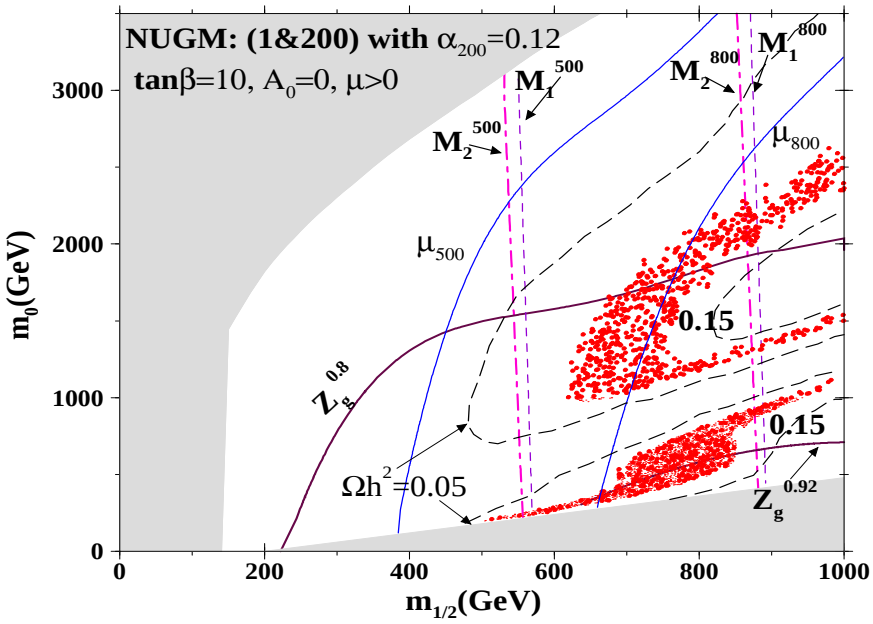

Figure 5: Allowed and disallowed zones of the (1+200) model. The WMAP DM relic density satisfying regions are shown in red in the $m_0 - m_{1/2}$ plane for $\tan\beta = 10$, $A_0 = 0$, $\mu > 0$ corresponding to $\alpha_{200} = 0.12$ of Eq.14. The upper disallowed region (in gray) corresponds to no EWSB ($\mu^2 < 0$). The lower gray region corresponds to stau becoming the LSP. Contours are drawn for M_1, M_2, μ, Z_g and $\Omega_{CDM}h^2$.

of Fig.5, except for the lower edge, which corresponds to the lower branch. There is a thin line separating the two regions, which is barely visible in this figure. Note that the spin-independent scattering is dominated by the Higgs exchange, whose coupling to the neutralino DM is proportional to the product of its higgsino and gaugino components. Thanks to the presence of $10 - 20\%$ of higgsino component in this model (Fig.5), the spin-independent cross-section is large enough to be detectable at the proposed superCDMS experiment [31]. Fig.6(b) shows the model prediction for the spin-dependent cross-section of the DM on nucleon. This is dominated by the Z exchange whose coupling to the neutralino DM is proportional to the square of its higgsino component. The shaded (red) region covers the two WMAP relic density satisfying branches of Fig.5. Again most of this region corresponds to the upper branch, with only the lower edge corresponding to the lower branch. As in the case of the previous model, the spin-dependent cross-sections here is too small to be seen at direct detection experiments [33].

parameter	A	B	C	D
$m_{1/2}$	725	900	725	900
m_0	1450	1357	590	950
μ	792	983	846	1009
M_1	652	814	646	811
$m_{\tilde{\chi}_1^0}$	633	798	633	797
$m_{\tilde{\chi}_2^0}$	657	818	650	815
$m_{\tilde{\chi}_3^0}$	794	985	848	1011
$m_{\tilde{\chi}_4^0}$	822	1009	869	1032
$m_{\tilde{\chi}_1^+,\tilde{\chi}_2^+}$	643,818	807,1005	641,865	806,1028
$m_{\tilde{g}}$	1700	2045	1637	2017
$m_{\tilde{t}_1}$	1460	1649	1216	1540
$m_{\tilde{t}_2,\tilde{b}_1}$	1813,1801	2013,2001	1478,1452	1860,1843
$m_{\tilde{l}}$	1535−1555	1505−1530	800−830	1160−1190
$m_{\tilde{q}_{1,2}}$	2000−2050	2170−2240	1520−1600	1950 −2040
$m_A(\simeq m_{H^+}, m_H)$	1726	1799	1174	1546

Table 3: MSSM masses in GeV for a few sample parameter points for the $1 + 200$ model.

Similar to what was discussed in Section 4 a larger Higgsino content of the LSP for $1+200$ scenario makes indirect detection of high energy neutrinos interesting. Fig.7 shows the rate of the resulting muon events for the IceCube experiment. The upper and lower shaded (red) branches correspond to the respective WMAP satisfying branches of Fig.5, with a clearly visible separation between them. As in the previous model, one expects a detectable signal rate ≥ 10 events per year at the IceCube experiment.

Fig.8 shows the rates of the line and the contunuum γ-ray signal coming from DM pair annihilation at the galactic core assuming the NFW profile of DM distribution [35]. Fig.8(a) shows the signal rate of the line γ-rays coming from DM pair annihilation,$\tilde{\chi}\tilde{\chi} \to \gamma\gamma(\gamma Z)$ via W boson loop. Since the wino has a large Isospin gauge coupling, the resulting γ ray signal here is at least an order of magnitude larger than the previous model. The shaded (red) band corresponding to the WMAP satisfying region of this model, predicts a line γ-ray flux of $\sim 10^{-13}$ cm^{-2} s^{-1}. Several atmospheric Cerenkov experiments have reported γ-ray events [43–46] at higher rate than this, but with continuous power-law energy spectrum,

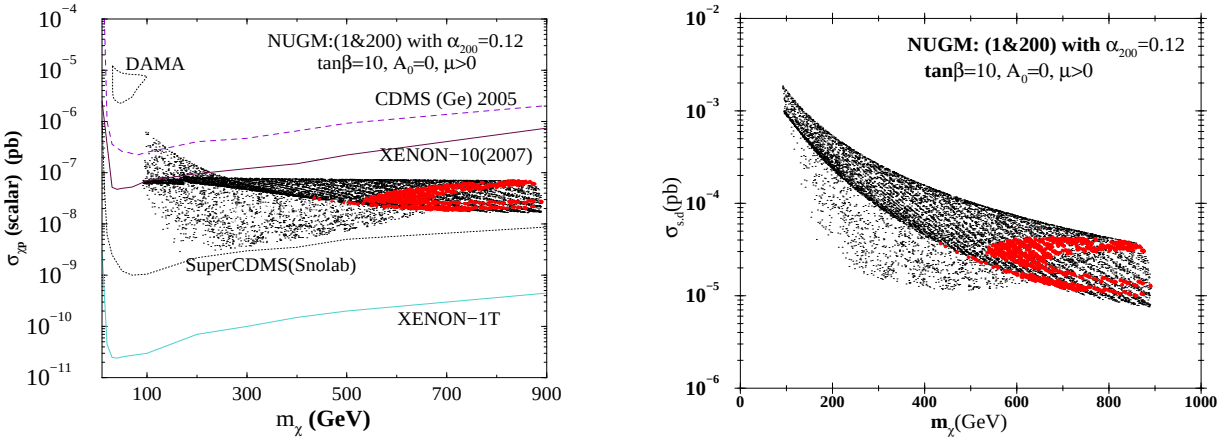

(a) (b)

Figure 6: (a): Spin-independent neutralino-proton cross section for the $(1 + 200)$ model vs. LSP mass for the parameters shown in Fig.5. The WMAP satisfied regions are shown in red. Various limits from the recent (DAMA, CDMS and XENON-10) and the future (SuperCDMS and XENON-1T) experiments are shown. (b): Spin-dependent neutralino-proton cross section for the $(1 + 200)$ model vs. LSP mass for the parameters shown in Fig.5. The WMAP satisfied regions are shown in red.

typical of supernova remnants. Therefore it will be hard to separate the DM signal from this background with the present energy and angular resolution of the ACT experiments.

Fig.8(b) shows the signal rate of the continuum γ-rays, coming from the tree-level pair annihilation processes of Eqs.16 and 17, with red dots corresponding to the WMAP satisfying regions. Since the most copious source of these γ rays is the b-quark jet from Eq. 17, the upper red dots correspond to the region of Fig.5 with large resonant annihilation contribution. Finally Fig.8(c) shows the continuum γ-ray spectrum for some representative points of this model, along with the discovery limit of the FGST/GLAST experiment [47]. It shows that a boost factor of $\sim 10^2$ to see this γ-ray signal in FGST/GLAST for the assumed NFW profile of DM distribution.

7 LHC Signatures of the $(1 + 75)$ and $(1 + 200)$ Models:

A quantitative investigation of the LHC signature of these two nonuniversal gaugino mass models is beyond the scope of this work. We shall only remark on some prominent features, which are quite evident from the SUSY spectra of Table 2 and 3. Table 2 clearly shows an

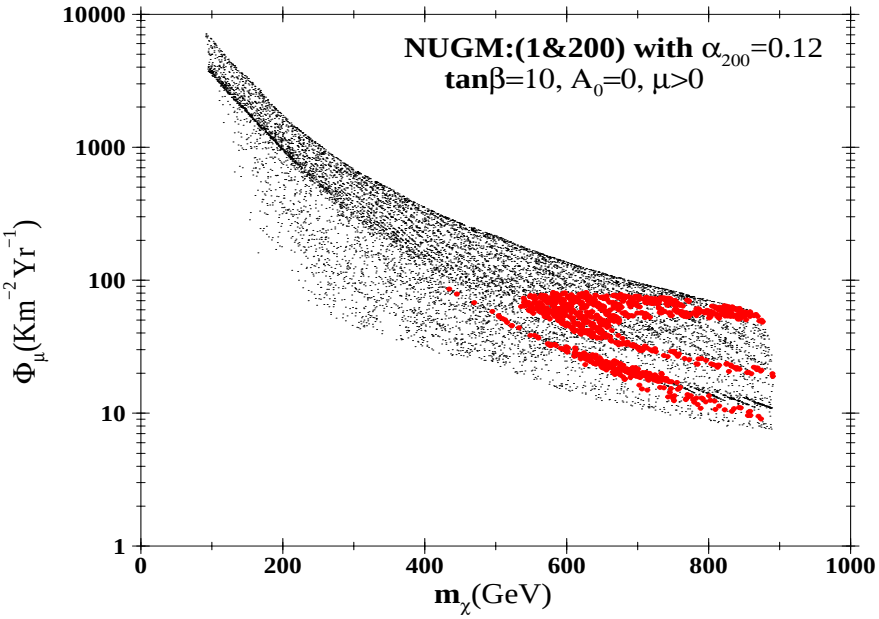

Figure 7: Neutralino annihilation induced muon flux from the Sun in $km^{-2}yr^{-1}$ vs LSP mass for the $(1+200)$ model for the parameters shown in Fig.5. The WMAP satisfied regions are shown in red.

inverted mass hierarchy for the $(1+75)$ model where the lighter stop is about 30% lighter than the 1st and 2nd generation squarks. Moreover it is lighter than the gluinos over most of the parameter space. So one expects a SUSY signal from the channels

$$pp \to \tilde{g}\tilde{g} \to tt\tilde{t}_1\tilde{t}_1, \quad pp \to \tilde{t}_1\tilde{t}_1 \tag{18}$$

inclusive of their antiparticles. In view of the singlet dominance of $\tilde{t}_1$, one expects it to decay via mainly gauge (Yukawa) coupling to $\tilde{B}(\tilde{H})$ into

$$\tilde{t}_1 \to t\chi^0_{1,2,3}, \quad b\tilde{\chi}^+_1. \tag{19}$$

Since all these neutralino and chargino states are nearly degenerate, we expect their p_T to be largely carried by the LSP(χ^0_1), giving relatively large missing-p_T ($\not{p}_T$) events along with soft jets (leptons). Note however that one expects hard leptons and b-jets from the decay of the top quarks in (18) and (19), resulting in hard and isolated multilepton+missing p_T signal accompanied by 4(2) b-jets for the pair production of gluon (stop).

The SUSY spectra of Table 3 also shows an inverted hierarchy for the (1+200) model with the $\tilde{t}_1$ being much lighter than the other squarks. Moreover it is lighter than the gluino over

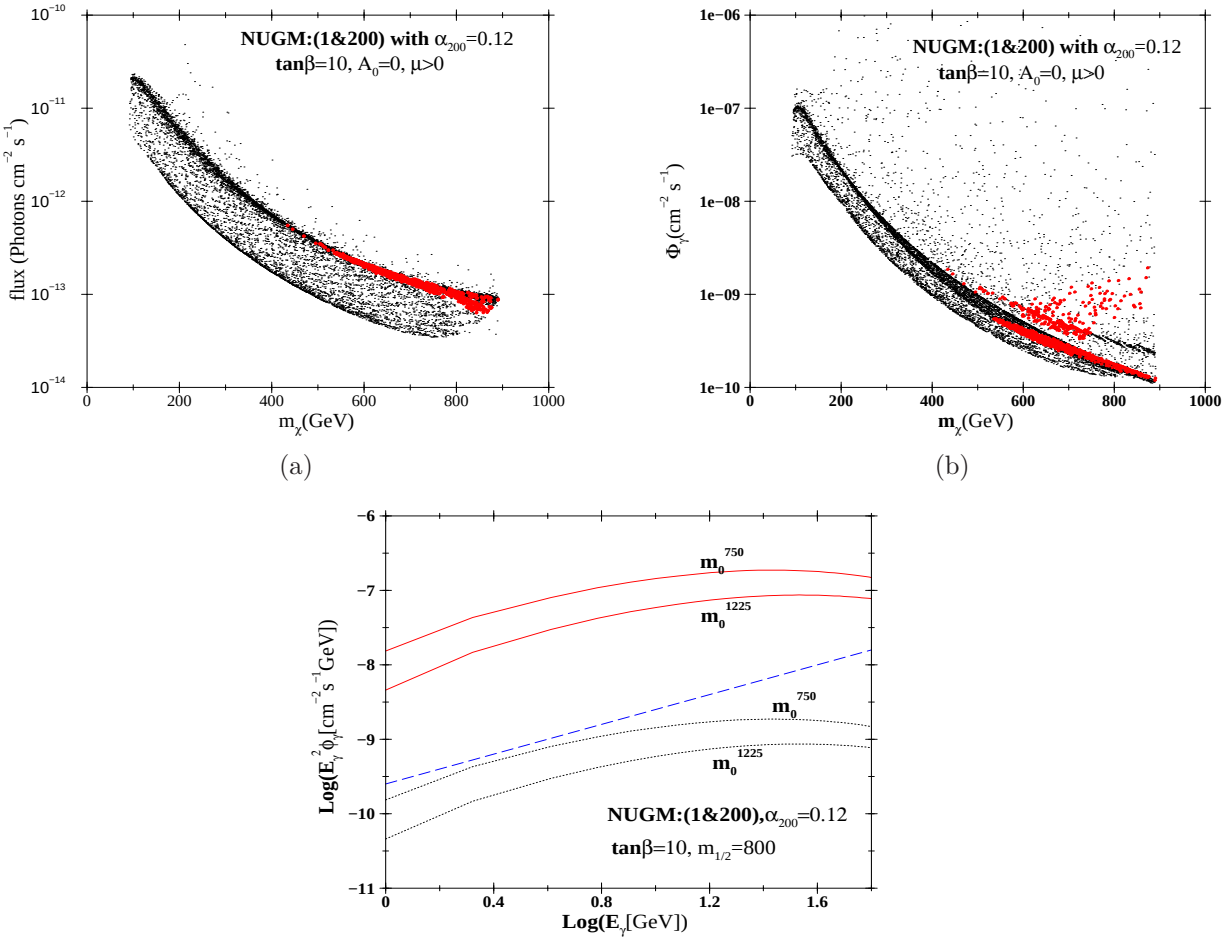

Figure 8: (a):Monochromatic γ-ray flux from DM pair annihilation near the galactic center vs. the LSP mass shown for the NFW profile of DM halo distribution and an aperture size of $\Delta\Omega = 10^{-3}$ sr for the $(1+200)$ Model. The parameters are same as in Fig.5. The WMAP satisfied regions are shown in red. (b): Same as (a) except that the vertical axis refers to a continuous γ-ray flux above a threshold energy of 1 GeV. (c): Photon spectra expected from two particular LSPs corresponding to $m_0 = 750$ GeV and $m_0 = 1225$ GeV for the $(1+200)$ Model with $m_{\frac{1}{2}} = 800$ GeV for an NFW profile. The other parameters are same as in Fig.5. The upper set of curves corresponds to a boost [36] factor of 10^2. The discovery limit of FGST/GLAST is shown as a blue straight line.

essentially the entire parameter space. Because of the rather heavy mass range of squarks and gluino in this model we expect a very important contribution to the LHC SUSY signal

to come from the pair production of $\tilde{t}_1$. Note that in this case the dominant decay channels are

$$\tilde{t}_1 \to t\chi^0_{1,2,3,4}, \quad b\tilde{\chi}^+_2, \tag{20}$$

since the higgsino dominated states are the heavier chargino and neutralino states $(\tilde{\chi}^+_2, \chi^0_{3,4})$. However these states are also quite close to the LSP χ^0_1 in this case. Therefore one expects signal characteristics as the earlier model. It should be mentioned here that similar characteristics of the LHC signal was noted for the focus point region of the mSUGRA model in [11], and has since been studied in detail in [12]. One expects similar features for these nonuniversal gaugino mass models of the mixed neutralino LSP as well. Only in these models one can have relatively light scalar mass m_0, so that the lighter $\tilde{t}_1$ is seen to be even lighter than the gluino, unlike the focus point case.

8 Conclusion

We have investigated the dark matter properties of non-universal gaugino mass scenarios where the gauge kinetic energy function is a mixture of chiral superfields that transforms as singlet and the 75-dimensional or the singlet and the 200 dimensional representation of SU(5). The mixing of the representaions are chosen so as to probe the dark matter annihilation properties of LSPs that are either a strong mixture of bino and Higgsinos in the 1+75 model or a mixture of bino-wino or even a mixture of bino-wino-higgsinos in the 1+200 model. For each of the scenarios we have analyzed the dark matter relic density in relation to the WMAP data and we have obtained broad regions of parameter space in the $m_0 - m_{\frac{1}{2}}$ plane that satisfy the WMAP data. We have identified the annihilation and coannihilation channels. We have further computed the direct detection rates of neutralino DM for the spin-independent and spin-dependent $\chi^0_1 - p$ cross sections. The spin-independent cross section ranges would be successfully probed in the near future via XENON-1T. We have also computed the neutralino-annihilation induced muon flux from the Sun that originates from the high energy neutrinos produced via pair-annihilation of LSPs in the solar core. We have found promising signals that will easily be probed in the IceCube experiment. We have also obtained interesting photon signal rates (both monochromatic and continuum) for the indirect detection of LSPs via γ-rays. FGST/GLAST will be able to probe a significant

region of parameter space with a possible boost factor. Finally, we have described a few distinctive features of the expected LHC signals of these models.

Acknowledgments

This work was initiated during the NORDITA Summer Programme (2008) at Stockholm. UC and DPR thank the organizers of this programme for their kind hospitality. The work of DPR was partially supported by BRNS (DAE) under the Raja Ramanna Fellowship Scheme. DD would like to thank the Council of Scientific and Industrial Research, Govt. of India for financial support.

References

[1] For reviews on Supersymmetry, see, eg, H. P. Nilles, Phys. Rep. **1**, 110 (1984); H. E. Haber and G. Kane, Phys. Rep. **117**, 75 (1985) ; J. Wess and J. Bagger, *Supersymmetry and Supergravity*, 2nd ed., (Princeton, 1991); M. Drees, P. Roy and R. M. Godbole, *Theory and Phenomenology of Sparticles*, (World Scientific, Singapore, 2005).

[2] A. H. Chamseddine, R. Arnowitt and P. Nath, Phys. Rev. Lett. **49**, 970 (1982); R. Barbieri, S. Ferrara and C. A. Savoy, Phys. Lett. B **119**, 343 (1982); L. J. Hall, J. Lykken and S. Weinberg, Phys. Rev. D **27**, 2359 (1983); P. Nath, R. Arnowitt and A. H. Chamseddine, Nucl. Phys. B **227**, 121 (1983); N. Ohta, Prog. Theor. Phys. **70**, 542 (1983); For reviews see [1] and P. Nath, R. Arnowitt and A.H. Chamseddine, *Applied N =1 Supergravity* (World Scientific, Singapore, 1984).

[3] C. Amsler *et al.* [Particle Data Group], Phys. Lett. B **667**, 1 (2008).

[4] E. Komatsu *et al.* [WMAP Collaboration], arXiv:0803.0547 [astro-ph].

[5] Physics at the CLIC Multi-TeV Linear Collider: CLIC Physics Working Group, [arXiv:hep-ph/0412251].

[6] U. Chattopadhyay, D. Das, P. Konar and D. P. Roy, Phys. Rev. D **75**, 073014 (2007); U. Chattopadhyay, D. Choudhury, M. Drees, P. Konar and D. P. Roy, Phys. Lett. B **632**, 114 (2006).

[7] N. Arkani-Hamed, A. Delgado and G. F. Giudice, Nucl. Phys. B **741**, 108 (2006), [arXiv:hep-ph/0601041].

[8] A. Masiero, S. Profumo and P. Ullio, Nucl. Phys. B **712**, 86 (2005).

[9] K. L. Chan, U. Chattopadhyay and P. Nath, Phys. Rev. D **58**, 096004 (1998); [arXiv:hep-ph/9710473]; U. Chattopadhyay, A. Corsetti and P. Nath, Phys. Rev. D **68**, 035005 (2003) [arXiv:hep-ph/0303201].

[10] J. L. Feng, K. T. Matchev and T. Moroi, Phys. Rev. D **61**, 075005 (2000); Phys. Rev. Lett. **84**, 2322 (2000); J. L. Feng, K. T. Matchev and F. Wilczek, Phys. Lett. B **482**, 388 (2000); J. L. Feng and F. Wilczek, Phys. Lett. B **631**, 170 (2005); U. Chattopadhyay, T. Ibrahim and D. P. Roy, Phys. Rev. D **64**, 013004 (2001).

[11] U. Chattopadhyay, A. Datta, A. Datta, A. Datta and D. P. Roy, Phys. Lett. B **493**, 127 (2000).

[12] E. Moulin *et al.*, Phys. Rev. D **77**, 055014 (2008); H. Baer, V. Barger, G. Shaughnessy, H. Summy and L. t. Wang, Phys. Rev. D **75**, 095010 (2007); S. P. Das, A. Datta, M. Guchait, M. Maity and S. Mukherjee, Eur. Phys. J. C **54**, 645 (2008), [arXiv:0708.2048 [hep-ph]].

[13] J. R. Ellis, K. Enqvist, D. V. Nanopoulos and K. Tamvakis, Phys. Lett. B **155**, 381 (1985); M. Drees, *ibid.* **158B**, 409 (1985).

[14] A. Corsetti and P. Nath, Phys. Rev. D **64**, 125010 (2001).

[15] U. Chattopadhyay and P. Nath, Phys. Rev. D **65**, 075009 (2002) [arXiv:hep-ph/0110341].

[16] G. Anderson, C.H. Chen, J.F. Gunion, J. Lykken, T. Moroi, and Y. Yamada, hep-ph/9609457; G. Anderson, H. Baer, C.H. Chen, and X. Tata, Phys. Rev. **D61**, 095005 (2000); K. Huitu, Y. Kawamura, T. Kobayashi, and K. Puolamaki, Phys. Rev. **D61**, 035001 (2000).

[17] U. Chattopadhyay and D. P. Roy, Phys. Rev. D **68**, 033010 (2003).

[18] S. F. King, J. P. Roberts and D. P. Roy, JHEP **0710**, 106 (2007) [arXiv:0705.4219 [hep-ph]].

[19] U. Chattopadhyay, D. Choudhury and D. Das, Phys. Rev. D **72**, 095015 (2005); U. Chattopadhyay, A. Corsetti and P. Nath, Phys. Rev. D **66**, 035003 (2002); S. Bhattacharya, A. Datta and B. Mukhopadhyaya, JHEP **0710**, 080 (2007); S. Bhattacharya, A. Datta and B. Mukhopadhyaya, arXiv:0804.4051 [hep-ph]; K. Huitu, J. Laamanen, P. N. Pandita and S. Roy, Phys. Rev. D **72**, 055013 (2005); G. Belanger, F. Boudjema, A. Cottrant, A. Pukhov and A. Semenov, Nucl. Phys. B **706**, 411 (2005) [arXiv:hep-ph/0407218].

[20] K. Huitu, R. Kinnunen, J. Laamanen, S. Lehti, S. Roy and T. Salminen, Eur. Phys. J. C **58**, 591 (2008) [arXiv:0808.3094 [hep-ph]].

[21] K. Choi, K. Y. Lee, Y. Shimizu, Y. G. Kim and K. i. Okumura, JCAP **0612**, 017 (2006); C. Pallis, Nucl. Phys. B **678**, 398 (2004).

[22] L. E. Ibanez, C. Lopez and C. Munoz, Nucl. Phys. B **256**, 218 (1985); L. E. Ibanez and C. Lopez Nucl. Phys. B **233**, 511 (1984).

[23] M. Carena, M. Olechowski, S. Pokorski, and C.E. Wagner, Nucl. Phys. **B426**, 269 (1994); S. Komine and M. Yamaguchi, Phys. Rev. **D63**, 035005 (2001).

[24] R. Barate *et al.* [LEP Working Group for Higgs boson searches], Phys. Lett. B **565**, 61 (2003) [arXiv:hep-ex/0306033].

[25] A. Djouadi, J. L. Kneur and G. Moultaka, arXiv:hep-ph/0211331.

[26] G. Belanger, F. Boudjema, A. Pukhov and A. Semenov, Comput. Phys. Commun. **176**, 367 (2007) [arXiv:hep-ph/0607059].

[27] P. Gondolo, J. Edsjo, P. Ullio, L. Bergstrom, M. Schelke and E. A. Baltz, JCAP **0407**, 008 (2004) [arXiv:astro-ph/0406204].

[28] A similar resonant annihilation zone in a small $\tan\beta$ scenario may be possible via non-universal scalar masses in the following reference. U. Chattopadhyay and D. Das, arXiv:0809.4065 [hep-ph].

[29] D. S. Akerib *et al.* [CDMS Collaboration], Phys. Rev. Lett. **96**, 011302 (2006) [arXiv:astro-ph/0509259]

[30] J. Angle *et al.* [XENON Collaboration], Phys. Rev. Lett. **100**, 021303 (2008) [arXiv:0706.0039 [astro-ph]].

[31] `http://www.fermilabtoday.com/directorate/program_planning/March2007PACPublic/CabreraPAC03_07.pdf;`
`For a limit plot see: http://dendera.berkeley.edu/plotter/entryform.html`

[32] `http://www.lngs.infn.it/lngs_infn/contents/lngs_en/research/experiments_scientific_info/experiments/current/xenon/collaboration.htm;`
`For a limit plot see : http://dendera.berkeley.edu/plotter/entryform.html`

[33] Z. Ahmed *et al.* [CDMS Collaboration], Phys. Rev. Lett. **102**, 011301 (2009) [arXiv:0802.3530 [astro-ph]]; H. S. Lee. *et al.* [KIMS Collaboration], Phys. Rev. Lett. **99**, 091301 (2007) [arXiv:0704.0423 [astro-ph]].

[34] R. Abbasi [IceCube Collaboration], arXiv:0902.0131 [astro-ph.HE].

[35] J.F. Navarro, C.S. Frenk, S.D.M. White, Astrophys. J. 462 (1996) 563; J.F. Navarro, C.S. Frenk, S.D.M. White, Astrophys. J. 490 (1997) 493.

[36] G. Bertone and D. Merritt, Phys. Rev. D **72**, 103502 (2005) [arXiv:astro-ph/0501555]; For adiabatic compression effects see the following:
G. R. Blumenthal, S. M. Faber, R. Flores and J. R. Primack, Astrophys. J. **301**, 27 (1986); R. Jesseit, T. Naab and A. Burkert, Astrophys. J. Lett **571**, L89 (2002), arXiv:astro-ph/0204164; O. Y. Gnedin, A. V. Kravtsov, A. A. Klypin and D. Nagai, Astrophys. J. **616**, 16 (2004) [arXiv:astro-ph/0406247]; F. Prada, A. Klypin, J. Flix, M. Martinez and E. Simonneau, arXiv:astro-ph/0401512.

[37] A. Cesarini, F. Fucito, A. Lionetto, A. Morselli and P. Ullio, Astropart. Phys. **21**, 267 (2004) [arXiv:astro-ph/0305075].

[38] The Fermi Gamma Ray Space Telescope: http://www-glast.stanford.edu .

[39] A. Morselli, A. Lionetto, A. Cesarini, F. Fucito and P. Ullio [GLAST Collaboration], Nucl. Phys. Proc. Suppl. **113**, 213 (2002) [arXiv:astro-ph/0211327].

[40] J. Carr, G. Lamanna and J. Lavalle, Rept. Prog. Phys. **69**, 2475 (2006).

[41] B. Moore, T. Quinn, F. Governato, J. Stadel and G. Lake, Mon. Not. Roy. Astron. Soc. **310**, 1147 (1999) [arXiv:astro-ph/9903164].

[42] J. Binney and S. Tremaine, *Galactic Dynamics*, (Princeton University Press, Princeton, 1987).

[43] M. Errando *et al.*, arXiv:0901.3275 [astro-ph.HE].

[44] V. A. Acciari *et al.* [VERITAS Collaboration], arXiv:0901.4527 [astro-ph.HE].

[45] K. Tsuchiya et al. [CANGAROO-II Collaboration], Astrophys. J. **606**, L115 (2004).

[46] F. Aharonian *et al.* [HESS Collaboration], Astrophys. J. **636**, 777 (2006) [arXiv:astro-ph/0510397].

[47] G. B. Gelmini, Int. J. Mod. Phys. A **23**, 4273 (2008) [arXiv:0810.3733 [hep-ph]]; M. Gustafsson, E. Lundstrom, L. Bergstrom and J. Edsjo, Phys. Rev. Lett. **99**, 041301 (2007) [arXiv:astro-ph/0703512].